INTERNATIONAL JOURNAL FOR NUMERICAL METHODS IN FLUIDS
Int. J. Numer. Meth. Fluids 2010; **62**:211–236
DOI: 10.1002/fld.2204

Assessment and modification of sub-cell-fix method for re-initialization of level-set distance function

M. B. Sun[1,2], Z. G. Wang[2] and X. S. Bai[1,*,†]

[1]*Division of Fluid Mechanics, Lund University, P.O. Box 118, S-221 00 Lund, Sweden*
[2]*College of Aerospace and Materials Engineering, National University of Defense Technology, 410073, Changsha, China*

SUMMARY

Sub-cell-fix re-initialization method was proposed by Russo and Smereka (*J. Comput. Phys.* 2000; **163**: 51–67) as a modification to the re-distancing algorithm of Sussman *et al.* (*J. Comput. Phys.* 1994; **114**: 146–159) that determines the distance function from an interface known as the zero level-set. The principal goal of sub-cell-fix method is to compute the distance function of the cells adjacent to the zero level-set without disturbing the original zero level-set. Following the original work of Russo and Smereka, several improved sub-cell-fix schemes were reported in the literature. In this paper, we show that in certain situations almost all the previous sub-cell-fix schemes can disturb the zero level-set, and the accuracy would not improve when the CFL numbers are decreased. Based on the scheme of Hartmann *et al.* (*J. Comput. Phys.* 2008; **227**:6821–6845), we propose an improved sub-cell-fix scheme that can significantly increase the accuracy of sub-cell-fix method on problems that are challenging. The scheme makes use of a combination of the points adjacent to zero level-set surfaces and preserves the interface in a second-order accuracy. The new sub-cell-fix scheme is capable of handling large local curvature, and as a result it demonstrates satisfactory performance on several challenging test cases. Limitations of the schemes on highly stretched grids are illustrated. Copyright © 2009 John Wiley & Sons, Ltd.

Received 29 June 2009; Accepted 14 September 2009

KEY WORDS: re-initialization; distance function; level-set equation; sub-cell-fix method

1. INTRODUCTION

Level-set approach is widely used in different engineering applications for computing interface evolution, for example crystal growth, flame propagation, two-phase flows, solid–fluid–gas

---

*Correspondence to: X. S. Bai, Division of Fluid Mechanics, Department of Energy Sciences, Lund University, P.O. Box 118, S-221 00 Lund, Sweden.
†E-mail: xue-song.bai@energy.lth.se

Contract/grant sponsor: Swedish Research Council VR, SSF, and STEM through CeCOST
Contract/grant sponsor: China Natural Science Foundation; contract/grant number: 50428605
Contract/grant sponsor: CSC (China Scholarship Council)

interaction [1–3]. In the level-set approach, the interface, Σ, is commonly represented by the zero level-set ϕ_0 of a continuous level-set function, ϕ, defined in a domain $\Omega \subset \boldsymbol{R}^n$; i.e.

$$\phi_0 = \{(\mathbf{x}, t) : \phi(\mathbf{x}, t) = 0\}, \quad \mathbf{x} \in R^n, \ \ t \in R^+$$

For $n = 3$, the components of the coordinate vector can be denoted by $\mathbf{x} = (x, y, z)^{\mathrm{T}}$.

The level-set function ϕ is defined everywhere in the domain Ω. The evolution of interface Σ is governed by a propagation equation for ϕ,

$$\frac{\partial \phi}{\partial t} + \mathbf{f} \cdot \nabla \phi = 0 \tag{1}$$

where $\mathbf{f}$ is the interface velocity. In fluid flow field $\mathbf{f} = \mathbf{v} + s\mathbf{n}$, where $\mathbf{v}$ is the underlying flow velocity, s is the propagation velocity of the front relative to the flow in the normal direction to ϕ_0. The normal direction is defined by the outward normal vector,

$$\mathbf{n} = -\frac{\nabla \phi}{|\nabla \phi|}$$

Note that the level-set equation (1) is derived for the interface, i.e the zero level-set. To obtain level-set function in Ω, one can extend the interface velocity $\mathbf{f}$ to the entire Ω domain. Alternatively, one can extend the level-set function to the entire Ω domain directly, by the following so-called re-initialization equation

$$|\nabla \phi| = 1 \tag{2}$$

This is specially useful since the level-set function is now a signed distance to the zero level-set interface, which can be used to determine the distributions of physical properties, such as density and chemical species, across premixed flames [4, 5]. The solution of the hyperbolic Equation (2) is the so-called re-initialization process.

The boundary condition for the re-initialization equation (2) is $\phi = 0$ at the zero level-set. It is a challenging task to implement this condition, since the zero level-set is implicitly embedded in the Ω domain. Discretization of Equation (2) can sometimes yield significant numerical dissipation that usually manifests itself as the zero level-set interface being abnormally disturbed (moved) or a loss of mass/volume in cases of high curvature or in under-resolved regions. A re-distancing technique was introduced by Sussman *et al.* [6], in which the level-set function is re-initialized without explicitly using the zero-level-set. The idea in this approach is to iterate on the equation

$$\phi_\tau = \operatorname{sign}(\phi)(1 - |\nabla \phi|) \tag{3}$$

until steady solution is reached. The converged steady solution gives the signed distance function. A major drawback of Equation (3) is that the zero level-set is considerably disturbed and that this disturbance may increase with the increasing number of iterations. This leads to a significant loss of accuracy of level-set-based engineering models, for example in turbulent premixed combustion applications where the density field and mass conservation are very sensitive to the errors in the distance function.

Efforts to improve the accuracy of distance function in level-set methods have led to a variety of re-initialization methods different from the original redistancing algorithm [6]. Sussman *et al.* [7, 8] proposed a re-initialization method that aims to preserve the partial volume cut by the interface in each cell. The method showed improved accuracy over both the level-set-only method and the volume-of-fluid-only method; however, the reconstructed interface appears noisy and lacks time coherence as demonstrated by Losasso *et al.* [9]. It was also noted that the method performed differently when using different numerical discretization schemes [10], and in a test case with two different compressible fluids separated by a sharp interface, the method produced unphysical oscillations [11]. To circumvent these problems, several authors proposed modified approaches such as the ghost-fluid method [12, 13], the variable time step method [14], and a hybrid of the Eulerian level-set method and the Lagrangian particle-tracking method [15]. Sethian and Smereka [10] showed that the ghost-fluid method may not be able to satisfy conservation near the interface. The methods are unstable when the interface is very close to grid nodes, and the interface would likely move across the grid node in re-initialization. The particle-tracking level-set approach [15] showed satisfactory results; however, the computational effort is generally high.

Russo and Smereka [16] developed a so-called sub-cell-fix method to keep the original interface undisturbed by manipulating the level-set function in the stencils in the neighborhood of the zero level-set. This method opened a possibility of achieving high accuracy in the numerical solution of Equation (3). However, how to construct a suitable signed distance using the neighboring cells is not a straightforward task. Min and Gibou [17] found that the central difference scheme used by Russo and Smereka [16] led to unstable results when the interface is close to grid nodes and they proposed to use a second-order polynomial to represent the zero level-set. The polynomial was constructed based on a locally adaptive Cartesian grid. The method improves the accuracy of the re-initialization process, but the implementation is comprehensively complex. Nilsson and Bai [18] used an upwind discretization across the zero level-set and obtained stable solution. Hartmann *et al.* [19, 20] proposed a hybrid of central difference and upwind discretization across the zero level-set to stabilize the solutions. To ensure minimal disturbance to the zero level-set, Hartmann *et al.* [19, 20] proposed two alternative formulations that were shown to perform better than the several previous sub-cell-fix methods. As we will show below, Hartmann *et al.*'s method has difficulty in maintaining high accuracy in the non-uniform grid and in the 3D problems. We propose here an improved sub-cell-fix scheme following the approach of Hartmann *et al.* [19, 20]. The scheme shows improved performance in several challenging test cases.

This paper is organized as follows. A brief description of the level-set method is given in Section 2. Several alternatives of the sub-cell-fix methods and their results are described in Section 3, followed by a suggestion for improvements in Section 4. Numerical evaluation of the proposed schemes for 2D and 3D problems is presented in Section 5, and conclusions are given in Section 6.

2. DISCRETIZATION OF LEVEL-SET EQUATION

Consider a computational domain Ω for the discretization of level-set equation (1). Denote Δ_x, Δ_y, Δ_z as the mesh sizes in the Cartesian coordinates x, y, and z direction, respectively. The cells in Ω are denoted by $C_{i,j,k}$, where the subscripts indicate their discrete location in the computational grid. Following the notations of Hartmann *et al.* [19, 20], the subset Γ of cells that are adjacent to the zero level-set is defined by

$$\Gamma=\left\{C_{i,j,k}:\left(\prod_{i',j,k}^{i,j,k}\phi\leqslant 0\right)\vee\left(\prod_{i,j',k}^{i,j,k}\phi\leqslant 0\right)\vee\left(\prod_{i,j,k'}^{i,j,k}\phi\leqslant 0\right)\right\}$$

DOI: 10.1002/fld

where $\prod_{i',j,k}^{i,j,k}\phi=\phi_{i,j,k}\phi_{i',j,k}$ for any combination of integers

$$i'\in\{i+1,i-1\},\quad j'\in\{j+1,j-1\},\quad k'\in\{k+1,k-1\}$$

Since the level-set equation (1) is for the zero level-set only, the computational cost of solving the equation can be reduced by using a so-called narrow band technique. That is, considering a localized computational domain $\Omega_\phi\subset\Omega$ around the zero level-set interface [21], with all cells outside Ω_ϕ discarded. Let B denote the narrow band subset of cells $C_{i,j,k}$. The narrow band B is generated in each re-initialization pseudo-time step, whereas the subset Γ is updated only once before the re-initialization process.

The level-set equation (1) is integrated in time with a 3-step third-order accurate Runge–Kutta scheme [22],

$$\begin{aligned}\phi_0&=\phi^n\\ \phi_k&=\alpha_k\phi_0+\beta_k\phi_{k-1}-\gamma_k\Delta t L(\phi_{k-1}),\quad k=1,2,3\\ \phi^{n+1}&=\phi_3\end{aligned}$$

where the coefficients are $\boldsymbol{\alpha}=(0,\frac{3}{4},\frac{1}{3})$, $\boldsymbol{\beta}=(1,\frac{1}{4},\frac{2}{3})$, and $\boldsymbol{\gamma}=(1,\frac{1}{4},\frac{2}{3})$. The subscript k denotes the Runge–Kutta step, whereas the superscript n corresponds to the time step, with time step interval Δt. The operator $L(\phi)$ denotes the numerical approximation of the term $\mathbf{f}\cdot\nabla\phi$ in Equation (1). Fifth-order weighted essentially non-oscillatory (WENO) scheme [23] is used to discretize the spatial derivatives in the level-set equation.

3. RE-INITIALIZATION AND SUB-CELL-FIX APPROACH

3.1. *The sub-cell-fix approach*

The basic idea of Russo and Smereka's sub-cell-fix approach [16] is to determine the signed distance function in the subset Γ using a special 'fixing' algorithm, whereas the signed distance function outside Γ is determined in a similar way as that of Sussman *et al.* [6]. The goal is to minimize the unwanted disturbance to the zero level-set in the re-initialization process. Russo and Smereka's sub-cell-fix approach can be described as follows:

$$\phi_{i,j,k}^{\nu+1}=\begin{cases}\phi_{i,j,k}^{\nu}-\dfrac{\Delta\tau}{\Delta_{\mathrm{x}}}(\mathrm{sgn}(\tilde{\phi}_{i,j,k})|\phi_{i,j,k}^{\nu}|-d_{i,j,k}) & \text{if } C_{i,j,k}\in\Gamma\\ \phi_{i,j,k}^{\nu}-\Delta\tau\mathrm{sgn}(\tilde{\phi}_{i,j,k})|\nabla\phi_{i,j,k}^{\nu}|-1 & \text{if } C_{i,j,k}\in B\wedge C_{i,j,k}\notin\Gamma\end{cases}\tag{4}$$

where $\tilde{\phi}_{i,j,k}$ denotes the level-set function before the re-initialization, i.e. $\tilde{\phi}=\phi^{\nu=0}$ and

$$d_{i,j,k}=\frac{\tilde{\phi}_{i,j,k}}{([\partial_x\tilde{\phi}_{i,j,k}]^2+[\partial_y\tilde{\phi}_{i,j,k}]^2+[\partial_z\tilde{\phi}_{i,j,k}]^2)^{1/2}}\tag{5}$$

It can be shown that $d_{i,j,k}$ is the signed distance function to a second-order accuracy. After (4), (5) converging to a steady state, $\phi_{i,j,k}$ is the target value of the level-set function on $C_{i,j,k}\in\Gamma$ approximating the signed distance function. An alternative approach to iteratively determining the level-set function on the cells in Γ is to directly update $\phi_{i,j,k} = d_{i,j,k} (\forall C_{i,j,k} \in \Gamma)$. The iterative and the direct approaches were tested and no difference in the stability and the rate of convergence was found. Thus, the direct approach is used in this study. In both approaches, the second equation in (4) invokes a pseudo-time step $\Delta\tau$ that is different from the physical time step (Δt) in the level-set equation. A first-order spatial discretization and forward Euler integration in the pseudo-time τ [19] is used here.

Russo and Smereka [16] used a central difference scheme to evaluate the discrete derivatives $[\partial_\xi \tilde{\phi}_{i,j,k}]$, $\xi = \{x, y, z\}$ in Equation (5). For $\xi = x$,

$$[\partial_x \tilde{\phi}_{i,j,k}] = \frac{\tilde{\phi}_{i+1,j,k} - \tilde{\phi}_{i-1,j,k}}{x_{i+1,j,k} - x_{i-1,j,k}}$$

We refer Russo and Smereka's sub-cell-fix formulation as RS scheme.

As will be illustrated later, RS scheme is sometimes unstable. Nilsson and Bai [18] replaced the central difference by the following mixed upwind scheme, for $\xi = x$,

$$[\partial_x \tilde{\phi}_{i,j,k}] = \max\left(\left| \frac{\tilde{\phi}_{i+1,j,k} - \tilde{\phi}_{i-1,j,k}}{x_{i+1,j,k} - x_{i-1,j,k}} \right|, \left| \frac{\tilde{\phi}_{i+1,j,k} - \tilde{\phi}_{i,j,k}}{x_{i+1,j,k} - x_{i,j,k}} \right|, \left| \frac{\tilde{\phi}_{i,j,k} - \tilde{\phi}_{i-1,j,k}}{x_{i,j,k} - x_{i-1,j,k}} \right|, \varepsilon_x \right)$$

where $\varepsilon_x = 10^{-8}$ is a small numerical number. This formulation is referred hereafter as NB scheme.

Both RS and NB schemes cannot ensure a non-disturbance to the zero level-set. To a low-order approximation, non-disturbance may be obtained by freezing the $\phi_{i,j,k}$ values in Γ, i.e. $d_{i,j,k} = \tilde{\phi}_{i,j,k} (\forall C_{i,j,k} \in \Gamma)$. The level-set function adjacent to the zero level-set is not updated and re-initialization is executed using the second of Equation (4) in the grid points other than Γ in the narrow band B. If the zero level-set is recomputed using linear interpolation from the level-set function after the re-initialization procedure, it can be shown that the zero level-set is preserved. However, it is easy to note that the level-set function in Γ is not the signed distance function. This will introduce errors when derivatives of the level-set function are evaluated in the narrow band. This freezing level-set approach has been examined by Dupont and Liu [24]. Hereafter, it will be referred to as the DL scheme.

To improve the stability and the accuracy of the sub-cell-fix method, Hartmann *et al.* [19] recently proposed a hybrid of upwind and central difference schemes. Russo and Smereka's central scheme is replaced by an upwind discretization scheme across the zero level-set if the involving cells are not in the Γ; otherwise, central difference scheme is used to maintain high accuracy. The discretization scheme can be written in a general form (for the x direction) as

$$[\partial_x \tilde{\phi}_{i,j,k}] = \frac{\tilde{\phi}^{+}_{i,j,k} - \tilde{\phi}^{-}_{i,j,k}}{\max(x^{+}_{i,j,k} - x^{-}_{i,j,k}, \varepsilon_x)}$$

where $\varepsilon_x = 0.001\Delta_x$ and for $\xi = \{\tilde{\phi}, x\}$

$$\xi^{\pm}_{i,j,k} = \begin{cases} \xi_{i,j,k} & \text{if } C_{i\pm1,j,k} \notin \Gamma \vee (\Im \wedge \aleph) \\ \xi_{i\pm1,j,k} & \text{otherwise} \end{cases} \tag{6}$$

DOI: 10.1002/fld

Conditions ($\Im$) and ($\aleph$) are defined as follows:

$$(\Im)\quad \text{if } \left(\prod_{i-1,j,k}^{i+1,j,k}\phi<0\right)\wedge(|\Delta^{\pm}_{i,j,k}\phi+\varepsilon_x|<|\Delta^{\mp}_{i,j,k}\phi|)$$

$$(\aleph)\quad \text{if } (\Delta^{+}_{i,j,k}\phi\Delta^{-}_{i,j,k}\phi<0)\vee\left(\prod_{i-2,j,k}^{i-1,j,k}\phi<0\right)\vee\left(\prod_{i+2,j,k}^{i+1,j,k}\phi<0\right)$$

where $\Delta^{+}_{i,j,k}\phi=\phi_{i+1,j,k}-\phi_{i,j,k}$, $\Delta^{-}_{i,j,k}\phi=\phi_{i,j,k}-\phi_{i-1,j,k}$. The conditions ($\Im$) and ($\aleph$) are formulated to account for cases with multiple interfaces about to coalesce. We refer this scheme as HMS1.

Define a subset $S_{i,j,k}$ that contains the neighboring cells of $C_{i,j,k}$ across the zero level-set interface, i.e. $S_{i,j,k}=\{C_{(i,j,k)_\alpha}:\phi_{i,j,k}\phi_{(i,j,k)_\alpha}<0\}$, $\alpha=\{1,\ldots,M_{i,j,k}\}$, where $M_{i,j,k}$ is the number of cells in $S_{i,j,k}$. For the $M_{i,j,k}$ cells, one can compute signed distance to zero level-set as HMS1 (Equations (5), (6)).

$$d_{(i,j,k)_\alpha}=\frac{\tilde{\phi}_{(i,j,k)_\alpha}}{([\partial_x\tilde{\phi}_{(i,j,k)_\alpha}]^2+[\partial_y\tilde{\phi}_{(i,j,k)_\alpha}]^2+[\partial_z\tilde{\phi}_{(i,j,k)_\alpha}]^2)^{1/2}} \tag{7}$$

Hartmann *et al.* [19] suggested to use the following averaging:

$$d_{(i,j,k)^*}=\frac{\tilde{\phi}_{i,j,k}}{M_{i,j,k}}\sum_{\alpha=1}^{M_{i,j,k}}\left(\frac{d_{(i,j,k)_\alpha}}{\tilde{\phi}_{(i,j,k)_\alpha}}\right) \tag{8}$$

to approximate the signed distance function at cell $C_{i,j,k}$ if $C_{i,j,k}\in\mathbb{C}$, where subset $\mathbb{C}$ is defined as [20],

$$\begin{aligned}\mathbb{C}&=\{C_{i,j,k}\in\Gamma:\kappa_{i,j,k}\phi_{i,j,k}<0\vee(\kappa_{i,j,k}=0\wedge\phi_{i,j,k}<0)\}\\ \Re&=\{\Gamma\backslash\mathbb{C}\}\cup\{S_{i,j,k}:C_{i,j,k}\in\mathbb{C}\}\end{aligned} \tag{9}$$

in which $\kappa_{i,j,k}$ is the local curvature, $\kappa=\nabla\cdot\mathbf{n}$.

It has the same formal order of accuracy (second order) as the signed distance function $d_{(i,j,k)_0}$ on the $C_{i,j,k}$ cell computed using Equations (5) and (6), i.e.

$$d_{(i,j,k)_0}=\frac{\tilde{\phi}_{i,j,k}}{([\partial_x\tilde{\phi}_{i,j,k}]^2+[\partial_y\tilde{\phi}_{i,j,k}]^2+[\partial_z\tilde{\phi}_{i,j,k}]^2)^{1/2}} \tag{10}$$

In cells $C_{i,j,k}\in\Re$, the signed distance function is determined using $d_{(i,j,k)_0}$. To summarize, the eventual signed distance function in $C_{i,j,k}$ cell is determined as follows:

$$d_{i,j,k}=\begin{cases}d_{(i,j,k)_0} & \text{if } C_{i,j,k}\in\Re\\ d_{(i,j,k)^*} & \text{if } C_{i,j,k}\in\mathbb{C}\end{cases}$$

Hereafter this scheme is referred to as HMS2.

Hartmann *et al.* [19] proposed an alternative to the averaging scheme (7). The new scheme is similar to HMS2, except that Equation (8) is replaced by the following:

$$d_{(i,j,k)^*}=\tilde{\phi}_{i,j,k}\sum_{\alpha=1}^{M_{i,j,k}} d_{(i,j,k)_\alpha} \Bigg/ \sum_{\alpha=1}^{M_{i,j,k}} \tilde{\phi}_{(i,j,k)_\alpha} \tag{11}$$

This scheme is referred to as HMS3.

3.2. *Performance of previous sub-cell-fix schemes*

The performance of the above six sub-fix-cell schemes is evaluated using two test cases, a rotating slot-disk [25] and a self-propagating circle. The same test cases were used by Hartmann *et al.* [19] on uniform grids. Here, we will examine their performance on both the uniform and the non-uniform grids.

Case 1 (*rotation of a slot-disk*): The rotation of a 2D slot-disk [25] is driven by an advection flow. A slot of width 5 and length 25 is cut out of a disk centered at $(x, y)=(50,75)$ with a radius $r=15$ in a computational domain $\Omega=[0,100]\times[0,100]$. The slot-disk is rotated with a velocity $\mathbf{f}=(u, v)$, cf. Equation (1), where $u=\pi(50-y)/314$, $v=\pi(x-50)/314$. The zero level-set is the slot-disk surface. The surface is rotated at the speed (u, v) without self propagation. A full revolution is accomplished at $t=T=628$. A CFL number of 0.64 is used, which corresponds to a time step $\Delta t=0.5$ on a 256^2 cell uniform grid (the characteristic velocity is assumed to be 0.5). To evaluate the schemes on the non-uniform grid, we used a hyper-tangent function to generate a stretched grid shown in Figure 1. The finest cell is at the point $(x, y)=(30,30)$ with the cell size $\Delta x=\Delta y=0.2$. The coarsest grid is at the boundaries of the domain and the cell size is 0.84. Thus, the maximal cell aspect ratio is about 4.2. Δt on the non-uniform grids is kept the same as the corresponding ones on the uniform grids.

The results obtained using the sub-cell-fix schemes RS, NB, DL, HMS1, HMS2, HMS3 on the uniform grid and the non-uniform grid systems are shown in Figure 2. The domain shown in the figures corresponds to the white windows in Figure 1. The lines shown in the figures are the zero level-set at the initial state $(t=0)$ and after one revolution of the disk $(t=T)$. If there was no

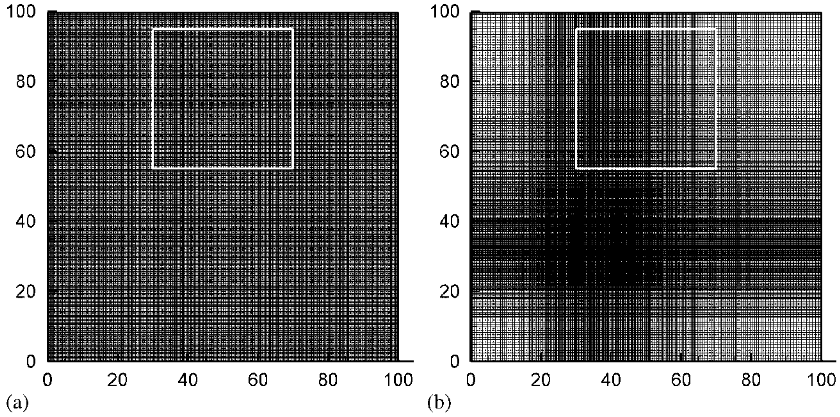

Figure 1. Grid systems for the rotating slot-disk case: (a) uniform grid and (b) non-uniform grid.

DOI: 10.1002/fld

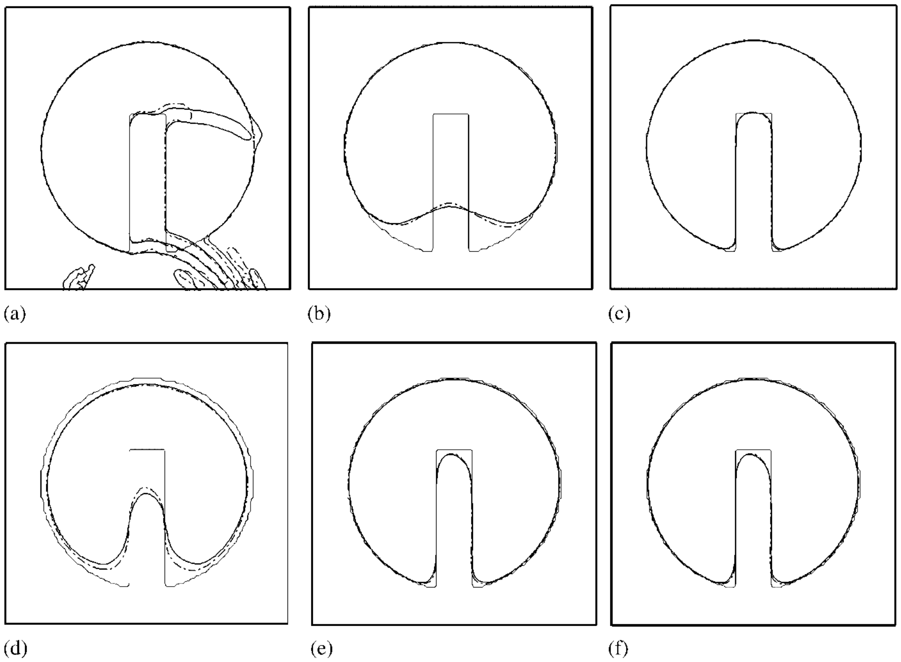

Figure 2. Rotating slot-disk after one revolution, simulated using the six sub-cell-fix schemes on 256^2 cell grids. Light solid lines: initial zero level-set; dark solid lines: results on the uniform grid; and dashdot lines: results on the non-uniform grid: (a) RS; (b) NB; (c) DL; (d) HMS1; (e) HMS2; and (f) HMS3.

disturbance in the re-initialization, the zero level-set at $t = T$ should be coincident with the initial zero level-set.

As noted, RS scheme results in unstable solution. The zero level-set at $t = T$ is noisy in several segments of the interface. NB scheme is rather stable; however, the slotted part of the disk is significantly smeared, indicating a strong disturbance to the zero level-set by the scheme. The HMS1 scheme is similar to the NB scheme with the result showing a smear of the slotted part of the disk. The results from DL, HMS2, HMS3 are more accurate than those from RS, NB, HMS1. The freezing level-set approach (DL) gives the smallest disturbance to the zero level-set. It is noted that for this rotating slot-disk case, the results from the uniform and the non-uniform grids are rather identical.

The influence of CFL number on the simulations is shown in Figure 3, where the results are obtained after one revolution of the slot-disk on the uniform grid using HMS1, HMS2, and HMS3. HMS1 becomes less accurate as CFL number decreases due to the fact that with smaller CFL number more pseudo-time steps are required in a rotation period, which results in more accumulated disturbance to the zero level-set. HMS2 and HMS3 are independent of the CFL number showing promising solution. The results from RS, NB, and DL are not shown in Figure 3; qualitatively, NB scheme gives results similar to that from HMS1; DL scheme does not disturb the zero level-set, and RS scheme is unstable with smaller CFL numbers.

Figure 4 shows results from HMS1, HMS2, and HMS3 after 1, 2, and 3 revolutions on the non-uniform grid. Similar to the case on the uniform grid, HMS1 shows accumulation of disturbance to

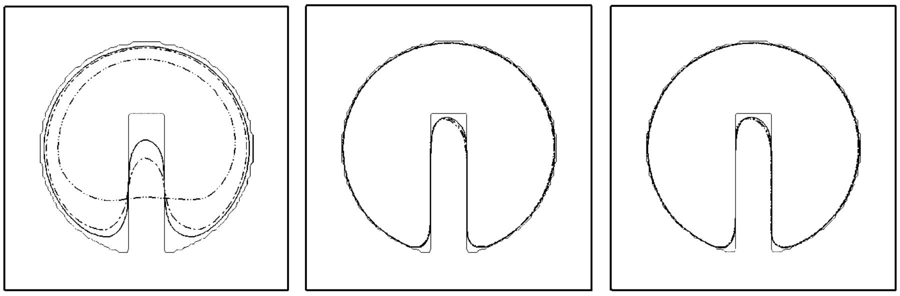

(a) (b) (c)

Figure 3. Rotating slot-disk after one revolution simulated on the uniform grid using the HMS schemes with different CFL numbers. Light solid lines: initial zero level-set; dark solid lines: CFL = 0.64; dashdot lines: CFL = 0.32; and dashdot-dot lines: CFL = 0.16: (a) HMS1 (b) HMS2; and (c) HMS3.

the zero level-set. The more revolution simulated the lower accuracy of the zero level-set. HMS2 and HMS3 perform better than HMS1. However, the disturbance to the zero level-set appears to accumulate slowly as more revolutions are simulated.

To quantify the disturbance of the sub-cell-fix schemes to the zero level-set and the accuracy of the signed distance function in the Γ subset, one can define the following two quantities: the mean displacement of zero level-set (ε_{ϕ_0}) and the mean deviation from the signed distance function (ε_Γ),

$$\begin{aligned}\varepsilon_{\phi_0} &= \frac{1}{N_\Gamma}\sum_{C_{ij}\in\Gamma}[(x(\phi_{i,j}=0)-x(\tilde{\phi}_{i,j}=0))^2+(y(\phi_{i,j}=0)-y(\tilde{\phi}_{i,j}=0))^2]^{1/2}\\ \varepsilon_\Gamma &= \frac{1}{N_\Gamma}\sum_{C_{ij}\in\Gamma}||\nabla\phi|_{i,j}-1|\end{aligned}\tag{12}$$

Figure 5 shows the mean displacement of the zero level-set and the mean deviation to the signed distance function by the HMS schemes on the uniform grid. HMS2 and HMS3 have the least disturbance to the zero level-set, whereas HMS1 has better accuracy in approximating the signed distance function in the Γ cells. As the disk rotates more, HMS2 and HMS3 yield increasing deviation from the signed distance function. HMS1 does not lead to increasing deviation to the signed distance function at later time. On the non-uniform grids, the same trend is seen in Figure 6. One major difference between the results from the uniform and the non-uniform grids is the periodic behavior of both the displacement of zero level-set and the deviation from the signed distance. This corresponds to the difference in grid resolution in regions where the zero level-set is located. At $t=0, T, 2T$, and $3T$ the disk is in the upper part of the domain where the grid is relatively coarse, yielding larger errors from the sub-cell-fix schemes. On contrary, when $t=T/2, 3T/2$, and $5T/2$, the disk is in the lower part of the domain where the grid is relatively fine; thereby, the HMS schemes yield smaller errors.

Case 2: self-propagating circle: Case 2 is a self-propagating circle without external convection [19]. The initial zero level-set (the initial shape of the circle) is a circle with radius $r=3$ centered at $(x, y)=(0,0)$ in a computational domain $\Omega=[-5,5]\times[-5,5]$. The zero level-set (the circle surface) satisfies the following level-set equation:

$$\frac{\partial\phi}{\partial t}=s_L|\nabla\phi|$$

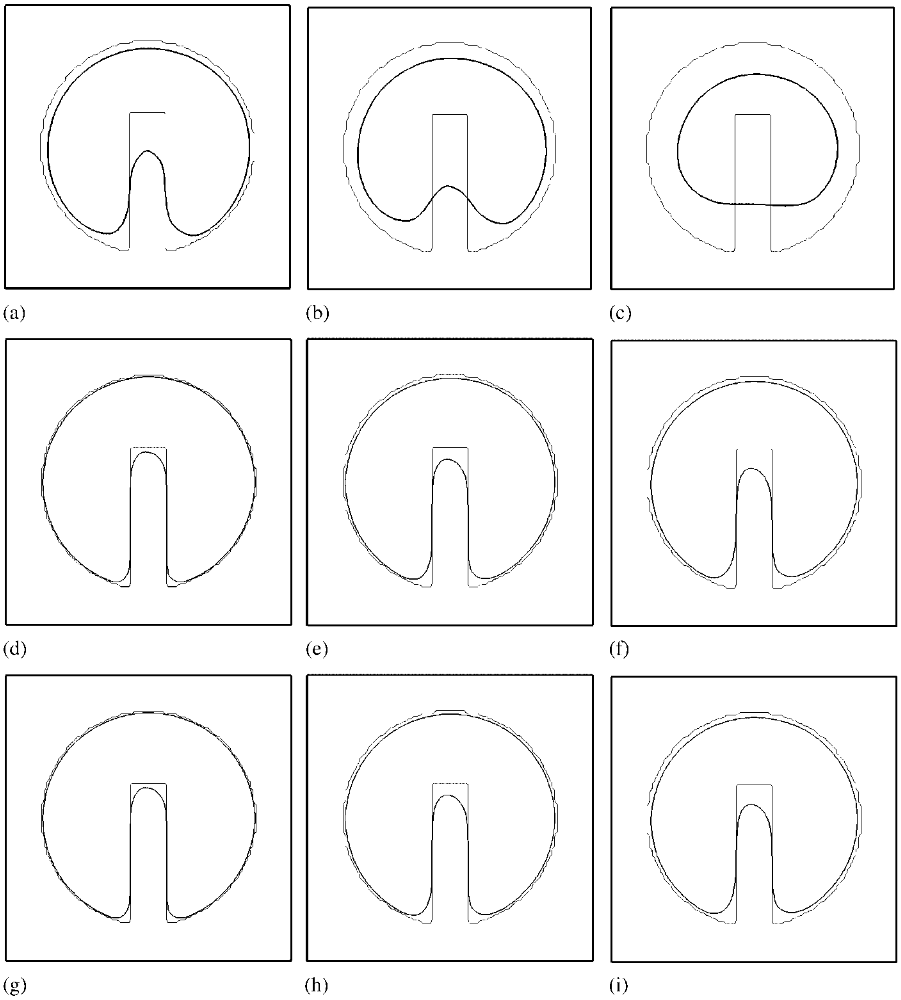

Figure 4. Rotating slot-disk after one, two, and three revolutions simulated using the HMS schemes on a 256^2 non-uniform grid. Light solid lines: initial zero level-set and dark solid lines: simulations: (a) HMS1, 1 revolution; (b) HMS1, 2 revolution; (c) HMS1, 3 revolution; (d) HMS2, 1 revolution; (e) HMS2, 2 revolution; (f) HMS2, 2 revolution; (g) HMS3, 1 revolution; (h) HMS3, 2 revolution; and (i) HMS3, 3 revolution.

where the self-propagation speed of the zero level-set (normal to the zero level-set) is defined by $s_L = \cos(8\Theta)\sin(\omega t)$, where $\Theta = \arctan|y/x|$, $\omega = 2\pi/T$, where $T = 5$ is the period during which the zero level-set oscillates from its initial position to its extreme and then returns to its initial position.

The simulations were carried out on a 256^2 uniform grid with a time step set as $\Delta t = 0.25\Delta x = 9.77\times 10^{-3}$. Figure 7 shows the zero level-set at $t = 0, T/2$, and T. As seen, at $t = T/2$, the zero level-set developed to finger-like shape with large local curvature. All schemes were shown to be

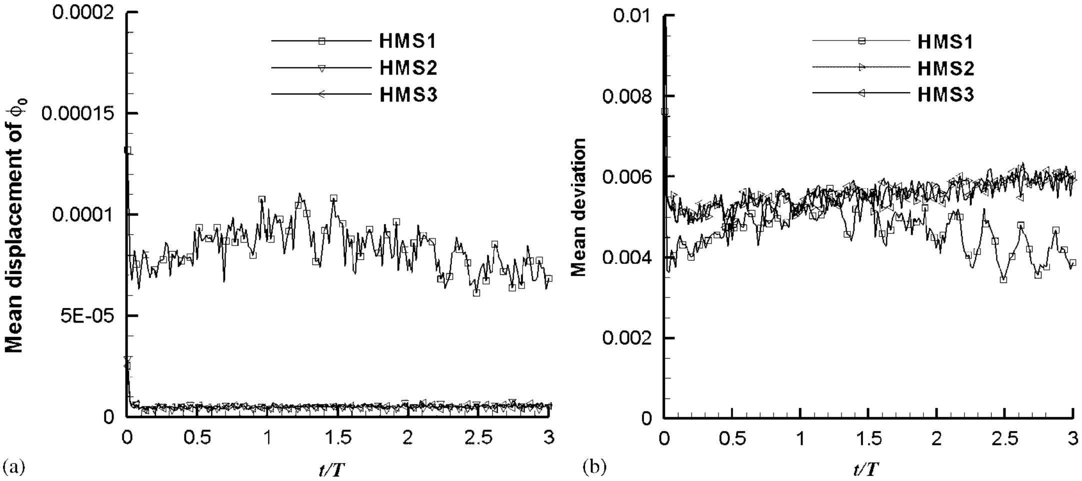

Figure 5. Numerical errors introduced by the HMS schemes on the 256^2 uniform grid for the rotating slot-disk case: (a) mean displacement of the zero level set and (b) mean deviation from $|\nabla\phi| = 1$ on cells in Γ. The data are plotted for each fifth time step.

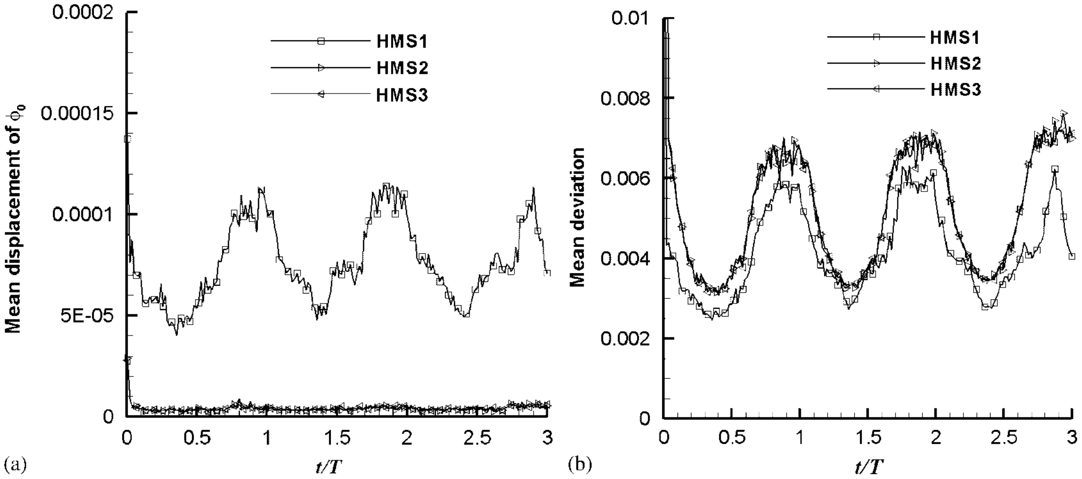

Figure 6. Numerical errors introduced by the HMS schemes on the 256^2 non-uniform grid for the rotating slot-disk case: (a) mean displacement of the zero level set and (b) mean deviation from $|\nabla\phi| = 1$ on cells in Γ. The data are plotted for each fifth time step.

stable. The difference of zero level-sets computed from different schemes is fairly small. However, when returning to its initial position at $t = T$, a large discrepancy among the results from the different schemes is shown. The results from RS, NB, DL, and HMS1 schemes are less accurate with a small-scale wrinkling in the zero level-set seen clearly. The results from HMS2 and HMS3 are satisfactory with its zero level-set graphically identical to the initial ones. It is interesting to

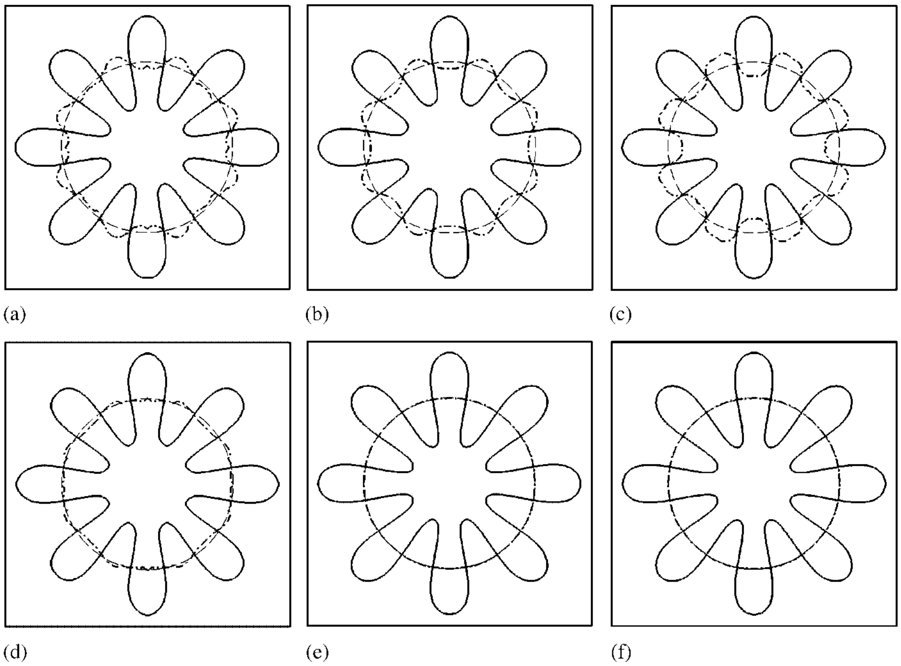

Figure 7. Self-propagating circle with space-dependent and time-dependent speed simulated using different sub-cell-fix schemes on a 256^2 uniform grid. Dash lines: intial zero level-set ($t=0$); solid lines: zero level-set at $t=T/2$; and dashdot lines: zero level-set $t=T$: (a) RS; (b) NB; (c) DL; (d) HMS1; (e) HMS2; and (f) HMS3.

note that the DL scheme that freezes the level-set function in Γ yields the largest error in the self-propagating-circle case, in contrary to its excellent performance in the rotating slot-disk case. It appears that with self-propagation of zero level-set taking into account the freezing zero level-set approach cannot ensure non-disturbance to the zero level-set. This can be attributed to the fact that the right-hand-side of the level-set equation requires evaluation of the gradient of level-set function, which involves the level-set function outside Γ.

Similar to the rotating slot-disk case, one can define the displacement of the zero level-set and the deviation from the signed distance function. In Figure 8, the mean displacement of the zero level-set and the mean deviation from $|\nabla\phi|=1$ are plotted for the different re-initialization schemes. The displacement of zero level-set by HMS2 and HMS3 is roughly of an order of magnitude smaller than that by HMS1. The deviation from the signed distance is rather similar for all HMS schemes. The displacement of the zero level-set by HMS2 and HMS3 goes to zero as the propagation speed goes to zero, i.e. at $t=0$, $t/2, T$. This is not the case for HMS1. The performance of the RS, NB, and DL schemes is similar to that of HMS1 (not shown in Figure 8 for brevity).

Next, we illustrate the performance of the sub-cell-fix schemes on the non-uniform grids. As shown in Figure 9(a), a non-uniform grid system with 256^2 cells is used with grid stretching starting from $(x, y)=(-2,-2)$ using the same hyper-tangent function as that for the rotating slot-disk case. The finest grid cell size is at $(-2,-2)$ with $\Delta x=\Delta y=0.02$. The coarsest cells are on the four boundaries of the domain with the same cell size of 0.084. Therefore, the maximal cell aspect ratio

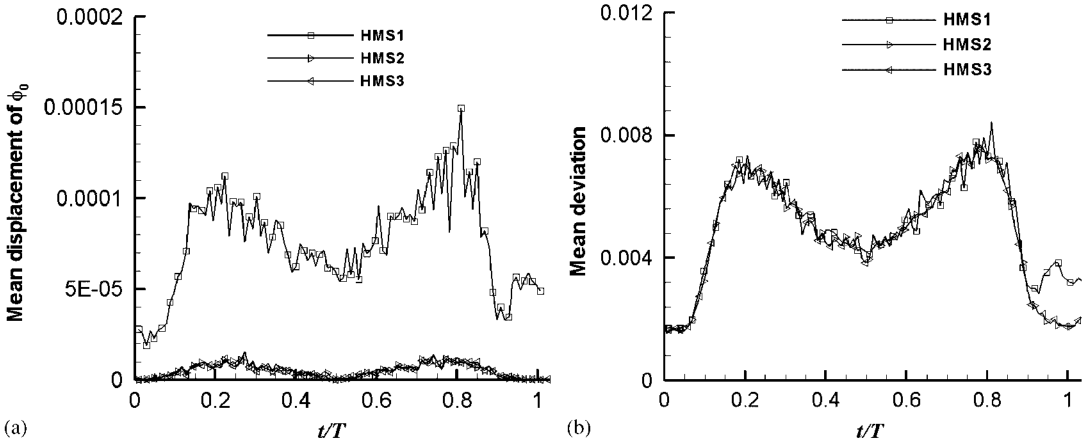

Figure 8. Numerical errors introduced by the HMS schemes on the 256^2 uniform grid for the self-propagating-circle case: (a) mean displacement of the zero level-set and (b) mean deviation from $|\nabla\phi| = 1$ on cells in Γ. The data are plotted for each fifth time step.

is also 4.2. Figures 9(b)–(f) show the zero level-set at $t = T/2$ and T. Time step is varied to illustrate the performance of different schemes on the non-uniform grids. The results with $\Delta t = 9.77\times10^{-3}$ are shown in Figures 9(b)–(c), and results with a smaller time step $\Delta t = 4.88\times10^{-3}$ are shown in Figures 9(d)–(f). All the sub-cell-fix schemes show certain disturbance to the zero level-set. HMS2 and HMS3 schemes that are rather accurate on the uniform grids yield severe disturbances to the zero level-set at $t = T$. With smaller time step the disturbance becomes larger, due to the fact that more executions of the sub-cell-fix procedure were performed with smaller time step. HMS1 and DL schemes perform similarly as they were on the uniform grids. Schemes RS and NB have similar performance as that of DL (not shown in Figure 9 for brevity).

In Figure 10, the mean displacement of the zero level-set and the mean deviation from $|\nabla\phi| = 1$ by the HMS schemes are plotted. Both the displacement and the deviation by HMS2 and HMS3 schemes become very large after $t = T/2$, whereas HMS1 yields relatively stable solutions.

To summarize, we note that none of the above sub-cell-fix schemes ensure non-disturbance to the zero level-set. With smaller time step in the numerical solution of level-set equation coupled with re-initialization, the numerical accuracy becomes worse due to the accumulation of disturbance to the zero level-set.

4. AN IMPROVED SUB-CELL-FIX SCHEME

To understand the source of disturbance to the zero level-set by the HMS schemes, we examine the different distance functions. Figure 11 schematically shows a 2D zero level-set in a rectangular non-uniform grid. Points $C_{i-1,j}$, $C_{i,j}$, $C_{i+1,j}$, $C_{i,j+1}$ are the neighboring ones of the zero level-set (curve ABC). For point $C_{i,j}$, there are two points in the $S_{i,j}$ sub-set: $C_{i-1,j}$ and $C_{i,j+1}$. Using Equations (5), (6), one can show that $d_{(i,j)_0}$ is the distance from $C_{i,j}$ to line AB, and $d_{(i,j+1)_0}$, $d_{(i-1,j)_0}$ are the distances from $C_{i,j+1}$ to line BC and from $C_{i-1,j}$ to line AD, respectively. It can be shown that $d_{(i,j)_1} = d_{(i,j+1)_0}\tilde{\phi}_{i,j}/\tilde{\phi}_{i,j+1}$ is the distance from $C_{i,j}$ to line BC, and

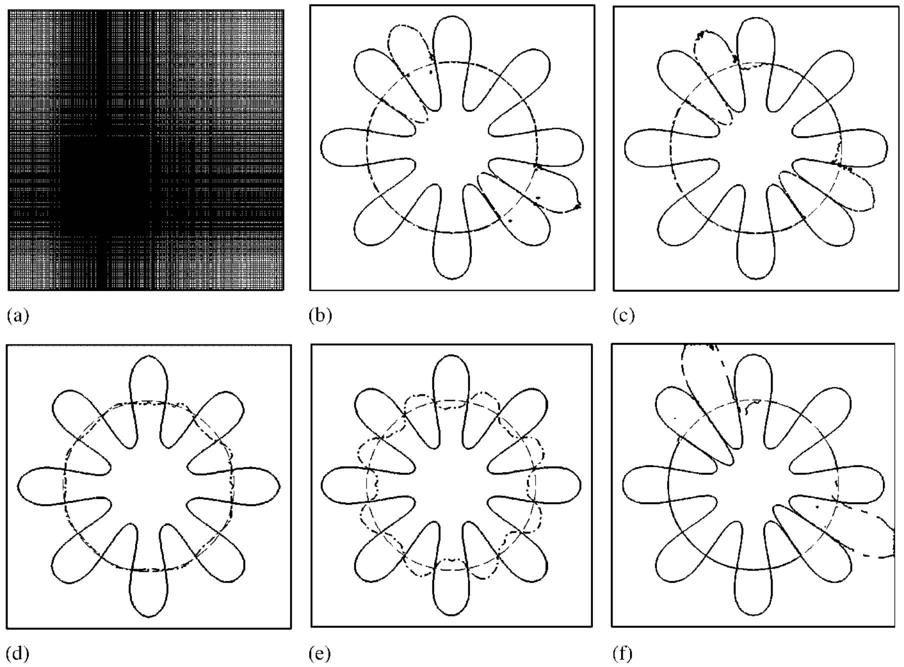

Figure 9. Self-propagating circle with space-dependent and time-dependent speed simulated on a 256^2 non-uniform grid using different sub-cell-fix schemes and time steps. (b)–(c): $\Delta t = 9.77\times10^{-3}$; (d)–(f): $\Delta t = 4.88\times10^{-3}$. Dashed lines: zero level-set at $t=0$; solid lines: zero level-set at $t=T/2$; and dashdotted lines: zero level-set at $t=T$: (a) non-uniform grid system; (b) HMS2; (c) HMS3; (d) HMS1; (e) DL; and (f) HMS2.

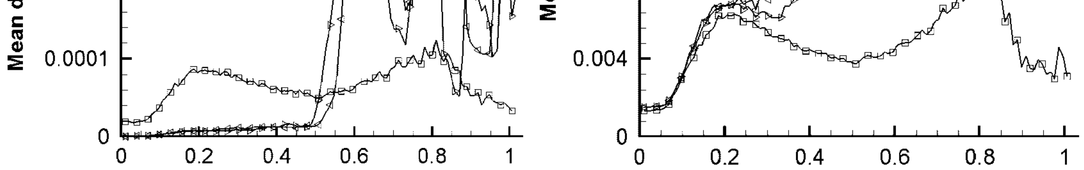

Figure 10. Numerical errors introduced by the HMS schemes on the 256^2 non-uniform grid for the self-propagating-circle case: (a) mean displacement of the zero level-set and (b) mean deviation from $|\nabla\phi| = 1$ on cells in Γ. The data are plotted for each fifth time step.

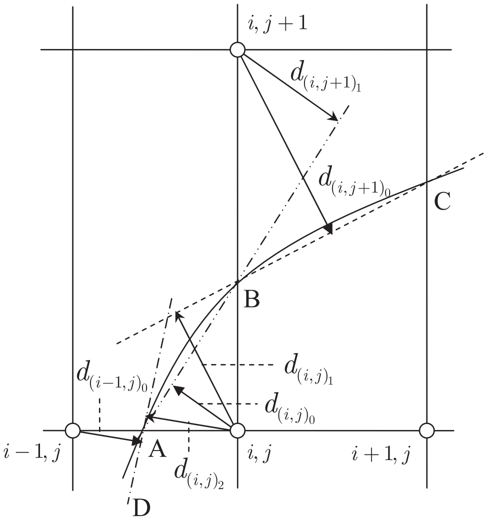

Figure 11. Schematic illustration of the different cells in the Γ subset and the different sub-cell-fix distances.

$d_{(i,j)_2}=d_{(i-1,j)_0}\tilde{\phi}_{i,j}/\tilde{\phi}_{i-1,j}$ is the distance from $C_{i,j}$ to line AD. For cell $C_{i,j}$, there are three signed distances, $d_{(i,j)_0}$, $d_{(i,j)_1}$, $d_{(i,j)_2}$, that can be used to determine the signed distance function $d_{i,j}$.

As illustrated in Figure 11, if one sets $d_{i,j}=d_{(i,j)_0}$ and $d_{i,j+1}=d_{(i,j+1)_0}$ the zero level-set point B is disturbed. Similarly, using other combinations the zero level-set would also be disturbed. It is easy to show that if the level-set is a line, then the different distance functions are identical to each other. From Figure 11, it appears that $C_{i,j}\in\Re$ whereas $C_{i-1,j}\in\mathbb{C}$ and $C_{i,j+1}\in\mathbb{C}$. This means that with HMS2 and HMS3 schemes, $d_{i,j}=d_{(i,j)_0}$ and $d_{i,j+1}=d_{(i,j+1)_1}$. B point is exactly preserved after the sub-cell-fix; however, zero level-set point C is not preserved. Further, we recall that the HMS2 and HMS3 schemes require computation of the curvature of the zero level-set. If errors accumulated in the zero level-set are so large that the sign of the curvature can be opposite, then the evaluation of the signed distance function by the HMS2 and HMS3 schemes uses different $d_{(i,j)_\alpha}$. The zero level-set point B may not be preserved after the sub-cell-fix.

To circumvent this problem, we propose to abandon the use of curvature. Similar to Hartmann *et al.* [19, 20] for the 3D problem, we define a subset $S_{i,j,k}$ that contains the neighboring cells of $C_{i,j,k}$ across the zero level-set interface, i.e. $S_{i,j,k}=\{C_{(i,j,k)_\alpha}:\tilde{\phi}_{i,j,k}\tilde{\phi}_{(i,j,k)_\alpha}<0\}$, $\alpha=\{1,\ldots,M_{i,j,k}\}$, where $M_{i,j,k}$ is the number of cells in $S_{i,j,k}$. We propose a modified sub-cell-fix scheme as follows:

1. for the cell $C_{i,j,k}$ in Γ, compute $d_{(i,j,k)_0}$ using HSM1 scheme;
2. for the cell $C_{i,j,k}$ in Γ, find the subset $S_{i,j,k}$;
3. for all the cells $\alpha=1,\ldots,M_{i,j,k}$ in $S_{i,j,k}$, compute $d_{(i,j,k)_\alpha}$ using the same scheme as HMS1;
4. further, for all the cells $\alpha=1,\ldots,M_{i,j,k}$ in $S_{i,j,k}$, compute the projected sub-cell-fix signed distance $d_{(i,j,k)^*}=\Phi(\tilde{\phi}_{i,j,k},\tilde{\phi}_{(i,j,k)_\alpha},d_{(i,j,k)_\alpha})$, in the same way as HMS2 or HMS3;
5. finally, for the cell $C_{i,j,k}$ in Γ, reconstruct signed distance $d_{i,j,k}$ using $d_{(i,j,k)_0}$ and $d_{(i,j,k)^*}$, by using the minimum of the two, i.e. $d_{i,j,k}=\min(d_{(i,j,k)^*},d_{(i,j,k)_0})$.

The rationale of step 5 is that, if $d_{(i,j,k)_\alpha}$ were small $\phi_{(i,j,k)_\alpha}$ would have low error. Thus, in order to increase the $\phi_{i,j,k}$ accuracy eventually, it is necessary to compare all $d_{(i,j,k)_\alpha}$ with one another and pick up the minimum one.

In the following, the above-modified sub-cell-fix schemes (steps 1–5) are referred to as the MSCF schemes. In particular, MSCF2 and MSCF3 correspond to the case that $d_{(i,j,k)^*}$ in step 4 is being determined using HMS2 and HMS3, respectively. MSCF1 corresponds to the case that $d_{i,j,k} = \min(d_{(i,j,k)_\alpha})$, $\alpha = 0, \dots M_{i,j,k}$, instead of steps 4 and 5.

5. PERFORMANCE OF THE MODIFIED SUB-CELL-FIX SCHEMES

5.1. *Order of the MSCF schemes*

The order of MSCF schemes can be demonstrated using a concentric circle test function [16, 19]. Assume that an initial level-set function has the form

$$\tilde{\phi}(\mathbf{x}) = g(\mathbf{x})(r - \sqrt{x^2 + y^2})$$

For $g(\mathbf{x}) = 1$, the function defines an infinite number of concentric circular level-sets with a zero level-set of radius r. Particularly, one may assume that $g(\mathbf{x})$ has the following form:

$$g(\mathbf{x}) = 0.1 + (x - r)^2 + (y - r)^2$$

The zero level-set in the initial field is a circle with radius r. Outside the zero level-set, the initial field is not a field of the signed distance function. If re-initialization is carried out, the level-set function would eventually converge to concentric circles i.e. signed distance function.

To quantify the order of the different schemes, an L_1-norm of the difference between the exact signed distance function ($D_{i,j} = r - \sqrt{x_{i,j}^2 + y_{i,j}^2}$) and the computed one ($\phi_{i,j}$) is determined in Γ by

$$e_1 = \|D - \phi\|_1 = \frac{1}{N_\Gamma} \sum_\Gamma |D_{i,j} - \phi_{i,j}|$$

where N_Γ is the number of cells in Γ. The results obtained on the uniform grids and the non-uniform grids (with various cell sizes) are summarized in Tables I and II, for the case that the zero level-set is a circle with radius $r = 3$. The computational domain is $\Omega = [-5, 5] \times [-5, 5]$. In the non-uniform grids, similar grid stretching as that in the self-propagating-circle case is used.

The accuracy of the HMS and MSCF schemes is shown in Figure 12. As seen, all schemes are second-order accurate on both the uniform and the non-uniform grids. The errors on the

Table I. L_1-norm of the difference between the exact signed distance function and the ones obtained from the HMS and MSCF schemes on the uniform grids.

Grid cells	HMS1	HMS2	HMS3	MSCF1	MSCF2	MSCF3
64^2	1.11×10^{-3}	1.24×10^{-3}	1.21×10^{-3}	1.44×10^{-3}	1.26×10^{-3}	1.21×10^{-3}
128^2	3.00×10^{-4}	3.04×10^{-4}	2.94×10^{-4}	3.76×10^{-4}	3.15×10^{-4}	2.98×10^{-4}
256^2	7.73×10^{-5}	7.58×10^{-5}	7.51×10^{-5}	9.34×10^{-5}	7.90×10^{-5}	7.51×10^{-5}

Table II. L_1-norm of the difference between the exact signed distance function and the ones obtained from the HMS and MSCF schemes on the non-uniform grids.

Grid cells	HMS1	HMS2	HMS3	MSCF1	MSCF2	MSCF3
64^2	5.53×10^{-3}	4.38×10^{-3}	4.37×10^{-3}	5.07×10^{-3}	4.99×10^{-3}	4.97×10^{-3}
128^2	9.80×10^{-4}	8.48×10^{-4}	8.32×10^{-4}	9.23×10^{-4}	8.89×10^{-4}	8.73×10^{-4}
256^2	8.98×10^{-5}	9.26×10^{-5}	9.09×10^{-5}	1.00×10^{-4}	9.35×10^{-5}	8.98×10^{-5}

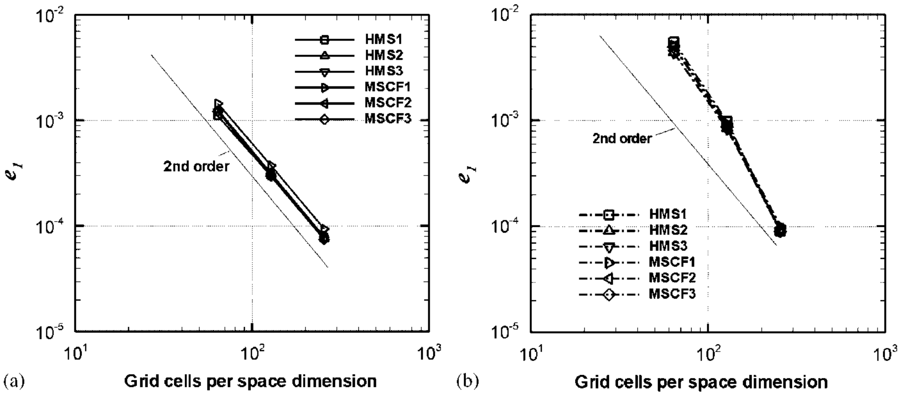

Figure 12. (a) Numerical errors introduced by the HMS and the MSCF schemes on (a) uniform grids and (b) non-uniform grids.

non-uniform coarse grids are generally higher than the corresponding ones on the uniform grids. On fine grids, the errors are of the same order on both the uniform and the non-uniform grids.

On the 256^2 non-uniform grids, the examination of the local error ($|D_{i,j}-\phi_{i,j}|$) distribution in Γ has shown that the largest error occurs in places with $\mathbf{n}\cdot\mathbf{i}=\frac{\sqrt{2}}{2}$. Here, $\mathbf{n}$ and $\mathbf{i}$ are the unity vectors normal to the zero level-set and along the x-axis, respectively. For $\mathbf{n}\cdot\mathbf{i}=0$ or 1, the zero level-set is nearly parallel to the grid lines, and the HMS and MSCF schemes yield smaller disturbance to the zero level-set.

The errors introduced by the different distance functions are shown to be a function of curvature of the zero level-set. For the radius of the zero level-set $r=3$, the maximal error is about 2.54×10^{-4} whereas for a smaller radius of $r=0.5$, the maximal error is about 5.88×10^{-4}, almost doubled.

Note that in this particular case, the zero level-set is fixed; hence, the cells in Γ are updated only once before the first iteration of the re-initialization step and remain unchanged thereafter. If the zero level-set evolves in time due to advection and self-propagation, the behavior of different sub-cell-fix schemes will be different as already seen in Section 3. This will be demonstrated further below.

5.2. *Test case 1*: *rotation of a slot-disk*

First, we examine the performance of the MSCF schemes in the rotating slot-disk case described in Section 3.2. The simulations were carried out on both the uniform and the non-uniform grids with 256^2 cells. The grids and the time steps are identical to the ones used in Section 3.2.

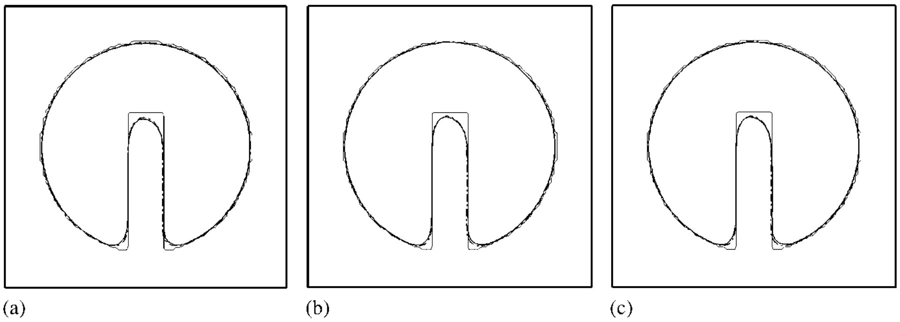

Figure 13. Rotating slot-disk simulated using the MSCF schemes on a 256^2 uniform grid and a non-uniform grid. Solutions are shown for one full revolution. Light solid lines: initial field; dark solid lines: solutions on the uniform grid; and dark dashdot lines: solutions on the non-uniform grid: (a) MSCF1; (b) MSCF2; and (c) MSCF3.

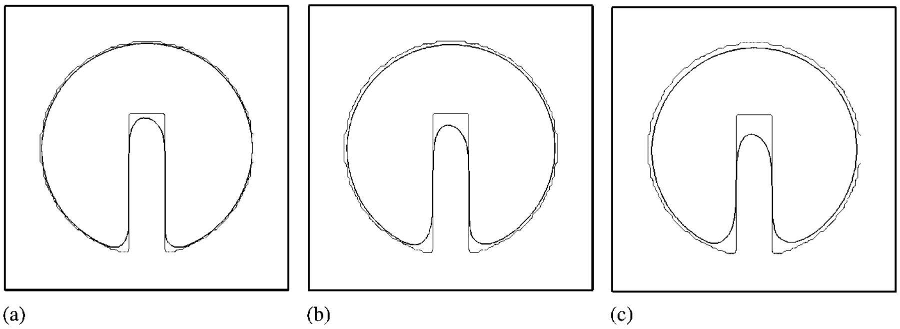

Figure 14. Rotating slot-disk simulated using the MSCF3 schemes on the 256^2 non-uniform grid. Solutions are shown for one full revolution (a); two full revolutions (b); and three full revolutions (c) of the disk. Light solid lines: initial field; dark solid lines: simulations.

As shown in Figures 13 and 14, and comparing with Figures 2–4, the MSCF schemes perform very well on this test case, with accuracy essentially similar to that of HMS3. The results on the uniform and the non-uniform grids are identical. The numerical errors introduced by the MSCF schemes are generally low and the difference between the schemes is small (cf. Figures 15 and 16). Similar to the HMS schemes, the displacement to the zero level-set and the deviation of the distance function by the three MSCF schemes show periodic variation on the non-uniform grid, owing to the varying local spatial resolution in places where the slot-disk is located.

5.3. *Test case 2*: *self-propagating circle on the non-uniform grids*

For the self-propagating-circle case discussed in Section 3.2, it was shown that the HMS schemes yield fairly large disturbance to the zero level-set when the non-uniform grids were used. Here, we consider the same non-uniform grid as the one used in Section 3.2, Figure 9(a). The time step

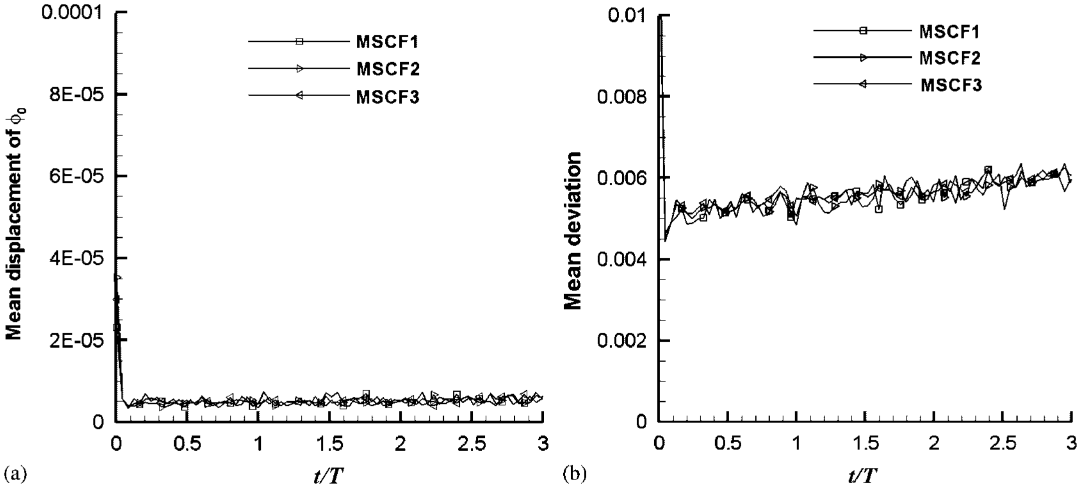

Figure 15. Numerical errors introduced by the MSCF schemes on the 256^2 uniform grid for the rotating slot-disk case: (a) mean displacement of the zero level set and (b) mean deviation from $|\nabla\phi| = 1$ on cells in Γ. The data are plotted for each fifth time step.

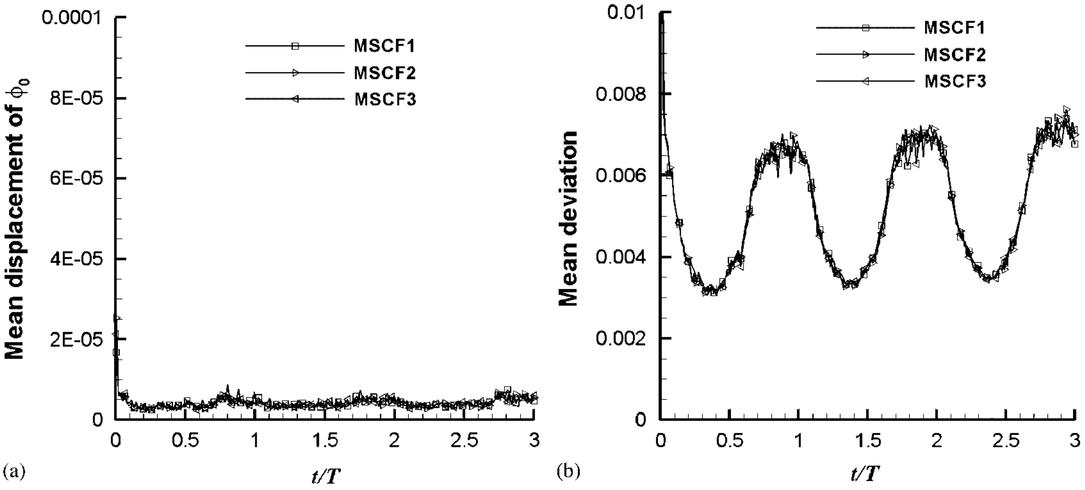

Figure 16. Numerical errors introduced by the MSCF schemes on the 256^2 non-uniform grid for the rotating slot-disk case: (a) mean displacement of the zero level set and (b) mean deviation from $|\nabla\phi| = 1$ on cells in Γ. The data are plotted for each fifth time step.

is $\Delta t = 0.125\Delta x$ on the uniform grid. For the non-uniform grid, Δt is kept the same as that on the uniform grids.

In Figure 17, the zero level-sets simulated using the MSCF schemes are plotted at $t = T/2$ and $t = T$, on a 256^2 uniform grid. As seen the three MSCF schemes yield satisfactory accuracy; the circular shape of the zero level-set can be well restored at $t = T$ on the uniform grids.

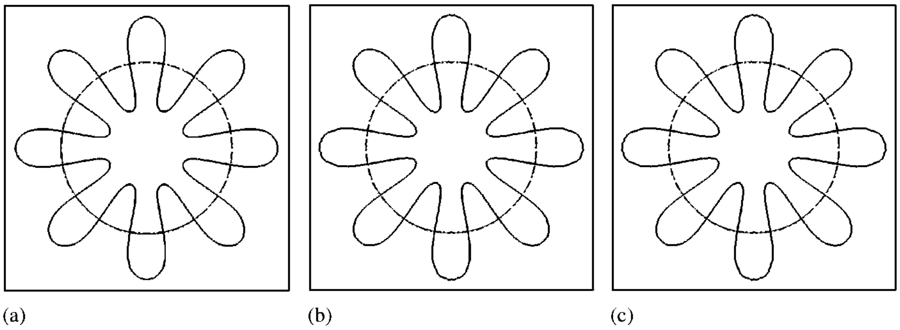

Figure 17. Self-propagating circle with space-dependent and time-dependent speed simulated using the MSCF schemes on a 256^2 uniform grid. Dashed lines: zero level-set at $t=0$; solid lines: zero level-set at $t=T/2$; and dashdotted lines: zero level-set at $t=T$: (a) MSCF1; (b) MSCF2; and (c) MSCF3.

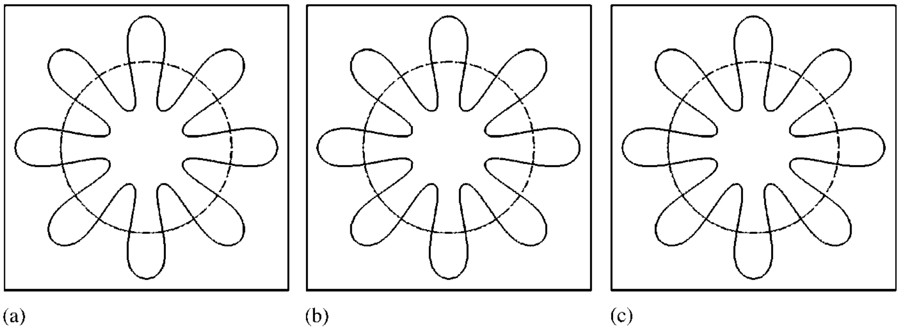

Figure 18. Self-propagating circle with space-dependent and time-dependent speed simulated using the MSCF schemes on a 256^2 non-uniform grid. Dashed lines: zero level-set at $t=0$; solid lines: zero level-set at $t=T/2$; and dashdotted lines: zero level-set at $t=T$: (a) MSCF1; (b) MSCF2; and (c) MSCF3.

In Figure 18, the zero level-sets at $t=T/2$, and $t=T$ obtained on a 256^2 non-uniform grid are shown. Comparing with Figure 9(f), the MSCF schemes are shown to yield much improved results on the non-uniform grid.

Figure 19 shows the mean displacement of the zero level-set and the mean deviation from $|\nabla\phi|=1$ computed using the MSCF schemes on the non-uniform grids. The MSCF schemes give a significantly improved solution on the non-uniform grid as compared with the HMS schemes.

5.4. Test case 3: coalescing and segregating circles

The third test case considered here is a case with two coalescing and segregating circles. The initial level-set function is given by

$$\phi(\mathbf{x})=\min(r-\sqrt{(x-a)^2+y^2}, r-\sqrt{(x+a)^2+y^2})$$

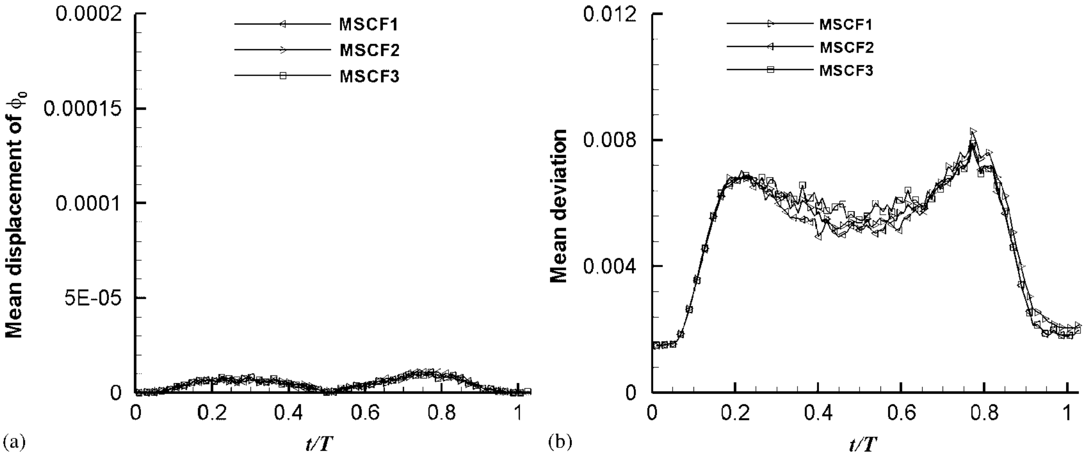

Figure 19. Numerical errors introduced by the MSCF schemes on the 256^2 non-uniform grid for the self-propagating-circle case: (a) mean displacement of the zero level-set and (b) mean deviation from $|\nabla\phi| = 1$ on cells in Γ. The data are plotted for each fifth time step.

with $r = 1.5$ and $a = 1.75$. The zero level-set is represented by two circles of radius $r = 1.5$ centered at $(x, y) = (-1.75, 0)$ and $(x, y) = (1.75, 0)$, respectively [19]. The computational domain $\Omega = [-5, 5] \times [-5, 5]$ is discretized using the 256^2 uniform and non-uniform grids. The non-uniform grid is identical to the one used in the self-propagating-circle case discussed in the previous section. The extension velocity is $\mathbf{f} = (1 - 2H(t-1))\mathbf{n}$, where H is Heaviside's step-function

$$H(t) = \begin{cases} 1, & t>0 \\ 0, & t<0 \end{cases}$$

To compare with the results of Hartmann *et al.* [19], the same small time step $\Delta t = 0.005$ used in [19] is employed here. With small time step, the number of re-initialization steps is large for the same time interval. This can lead to more significant difference between the re-initialization schemes.

In Figure 20, the zero level-set simulated using the HMS1, HMS2, MSCF1, and the MSCF2 schemes on the 256^2 uniform and non-uniform grids are plotted. It appears that on the uniform grids, the HMS2 and the MSCF schemes give fairly similar results. At the coalescing points of the circles cusps are shown to form with abrupt change of first derivative. The results from HMS1 and MSCF schemes are rather similar, with noticeable difference found only at rather later time $t>2.0$. On the non-uniform grids, however, the HMS2 scheme gives rather noisy zero level-set, whereas the MSCF schemes on the non-uniform grids are rather similar to that on the uniform grids.

The results from HMS3 are similar to that of HMS2; the results from MSCF3 are similar to that of MSCF2. For brevity, the results from HMS3 and MSCF3 were omitted in Figure 20.

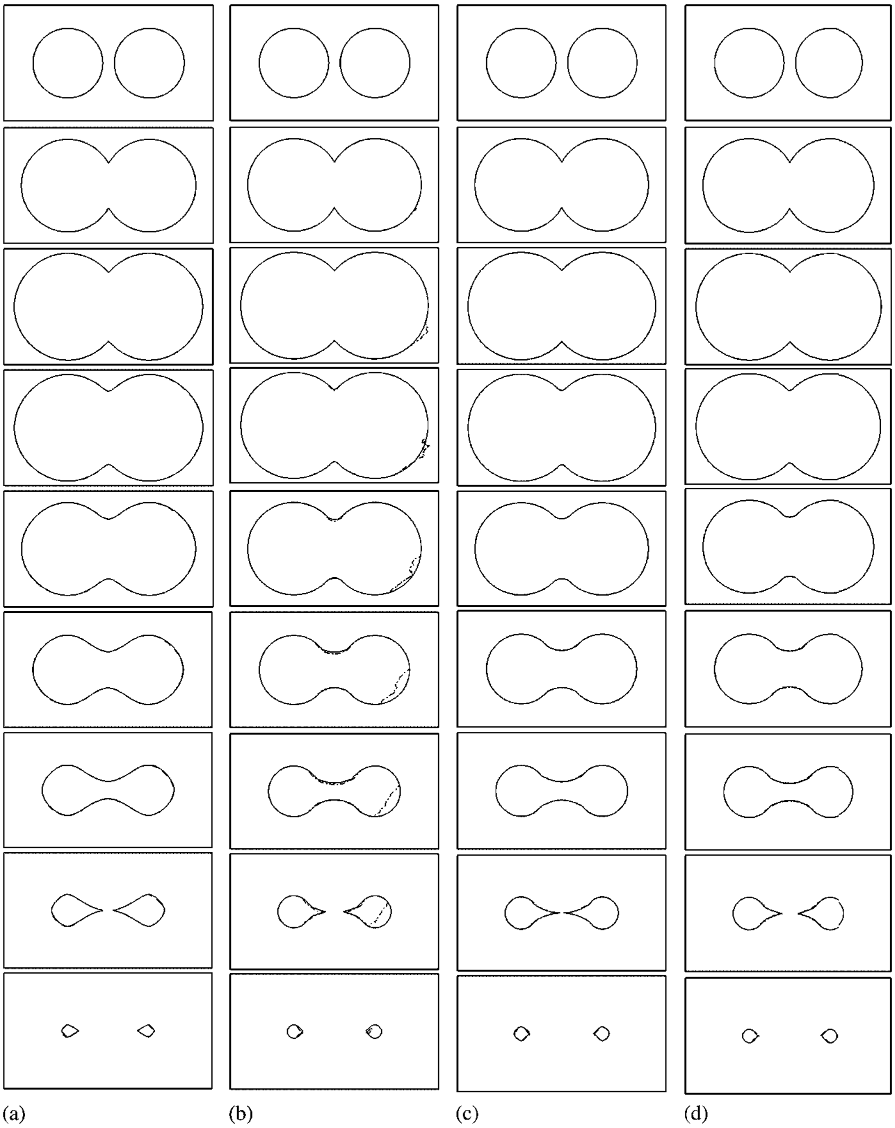

Figure 20. Coalescing and segregating circles simulated using the HMS and MSCF schemes on the 256^2 uniform and non-uniform grids. From top to bottom: $t=0$, $t=0.5$, $t=0.8$, $t=1.2$, $t=1.5$, $t=2.0$, $t=2.4$, $t=2.8$, $t=3.2$; solid lines, uniform grids; dashed lines, non-uniform grids: (a) HMS1; (b) HMS2; (c) MSCF1; and (d) MSCF2.

5.5. *Test case 4*: *coalescing and segregating spheres*

The case of coalescing and segregating spheres is a 3D extension of the coalescing and segregating circle case studied in Section 5.4. The initial level-set function is given by

$$\phi(\mathbf{x})=\min(r-\sqrt{(x-a)^2+y^2+z^2}, r-\sqrt{(x+a)^2+y^2+z^2})$$

DOI: 10.1002/fld

with $r=1.5$ and $a=1.75$. The zero level-set is the surface of two spheres of radius $r=1.5$, centered at $(x, y, z)=(-1.75, 0, 0)$ and $(1.75, 0, 0)$. The extension velocity is the same as that in Section 5.4. The computational domain $\Omega=[-5, 5]\times[-5, 5]\times[-5, 5]$ is discretized by the 128^3 uniform and non-uniform grids. The non-uniform grid has the same function form as the one used in the 2D test cases. The finest cell is at $(-2, -2, -2)$, whereas the coarsest cells are on the six boundary surfaces of the computational domain. Different levels of grid stretching were tested.

In Figures 21 and 22, the results on the uniform grids and the non-uniform grid with maximal aspect ratio of 2 are shown. Figure 21 shows the results obtained using HMS1 and HMS2. On the uniform grids, the HMS2 scheme yields reasonable results with well-preserved sphere shape in the coalescing stage, but noisy surfaces in the segregating stage ($t>2.4$). On the non-uniform grid with maximal cell aspect ratio of 2, the HMS2 scheme yields rather noisy results already at $t>0.5$, with the sphere shape greatly distorted. The results from HMS1 on the uniform grid and the non-uniform grid are fairly stable and identical, but the sphere surface cannot be preserved. This observation is consistent with the 2D calculation of Section 5.4 and the results reported in Hartmann *et al.* [19]. The results from HMS3 were not shown in the figure for brevity, which are similar to that of HMS2.

Figure 22 shows results obtained using MSCF1 and MSCF2. On the uniform grids, the MSCF1 and MSCF2 schemes both yield reasonable results with well-preserved sphere shape in both the coalescing and segregating stages. On the non-uniform grids, the MSCF1 scheme yields fairly good results in all stages, whereas the MSCF2 scheme shows somewhat noisy intersecting surfaces in the segregating stage ($t>1.2$). Nevertheless, one notices significant improvement of the MSCF schemes as compared with the HMS schemes. The results from MSCF3 are not shown in the figure for brevity. In general, the results from MSCF3 are similar to that of MSCF2.

Numerical experiments with higher cell aspect ratio (e.g. maximal cell aspect ratio of 4.2) shows that the HSM2, the HMS3, and the MSCF schemes become unstable, yielding noisy disturbance to the sphere surface. HMS1 scheme is stable on this high stretching non-uniform grid; however, the spherical surface is distorted and the spherical shape is not preserved. This behavior is even observed on the uniform grids as discussed above.

6. SUMMARY

An assessment is carried out on different sub-cell-fix schemes for re-initialization of the level-set function to the signed distance function. It is shown that sub-cell-fix schemes introduce disturbance to the zero level-set due to the unavoidable truncation errors. As a result, the zero level-set is either stable but smeared out, or unstable with growing non-physical disturbance to the zero level-set as the error appears to accumulate. With smaller time steps, the accumulated disturbance to the zero level-set is even more severe. Improvements to the sub-cell-fix schemes are discussed, and the improved sub-cell-fix schemes are proposed. The new formulation, referred here as the MSCF schemes, is based on the schemes of Hartmann *et al.* [19]. The schemes are evaluated for different test cases used in the previous literature, and also for more challenging 3D cases on both the uniform and the non-uniform grids.

On the 2D rotating slot-disk, self-propagating circle, and coalescing and segregating circles cases, the MSCF schemes yield significantly improved interface capture on both the uniform

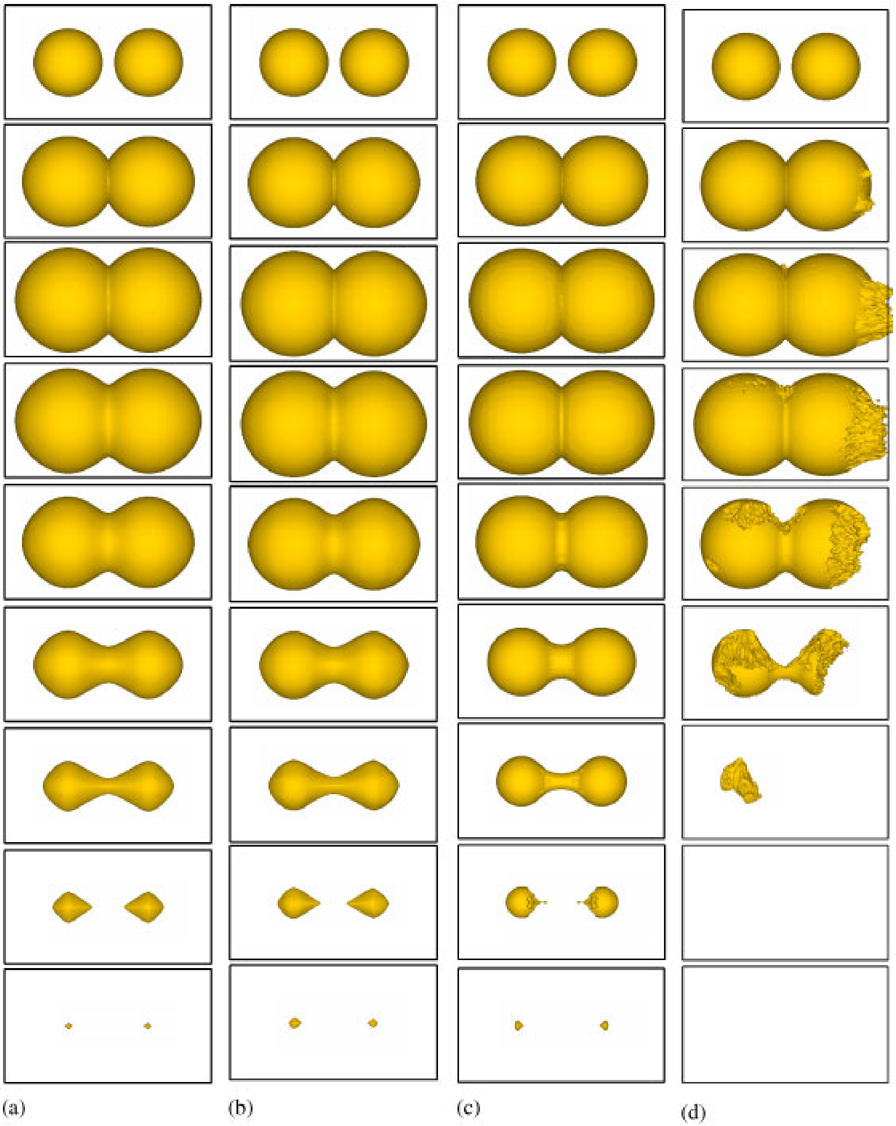

Figure 21. Coalescing and segregating spheres simulated using the HMS1 and HMS2 schemes on the 128^3 uniform and non-uniform grids. From top to bottom: $t=0$, $t=0.5$, $t=0.8$, $t=1.2$, $t=1.5$, $t=2.0$, $t=2.4$, $t=2.8$, $t=3.2$: (a) HMS1, uniform grid; (b) HMS1, non-uniform grid; (c) HMS2, uniform grid; and (d) HMS2, non-uniform grid.

and the non-uniform grids. The MSCF schemes simulated well-preserved zero level-set interface propagation for all the tested 2D cases that many previous sub-cell-fix schemes failed to capture.

On the most challenging 3D coalescing and segregating spheres case, the MSCF schemes, especially the MSCF1 scheme, perform well on the uniform grids and the moderately stretched

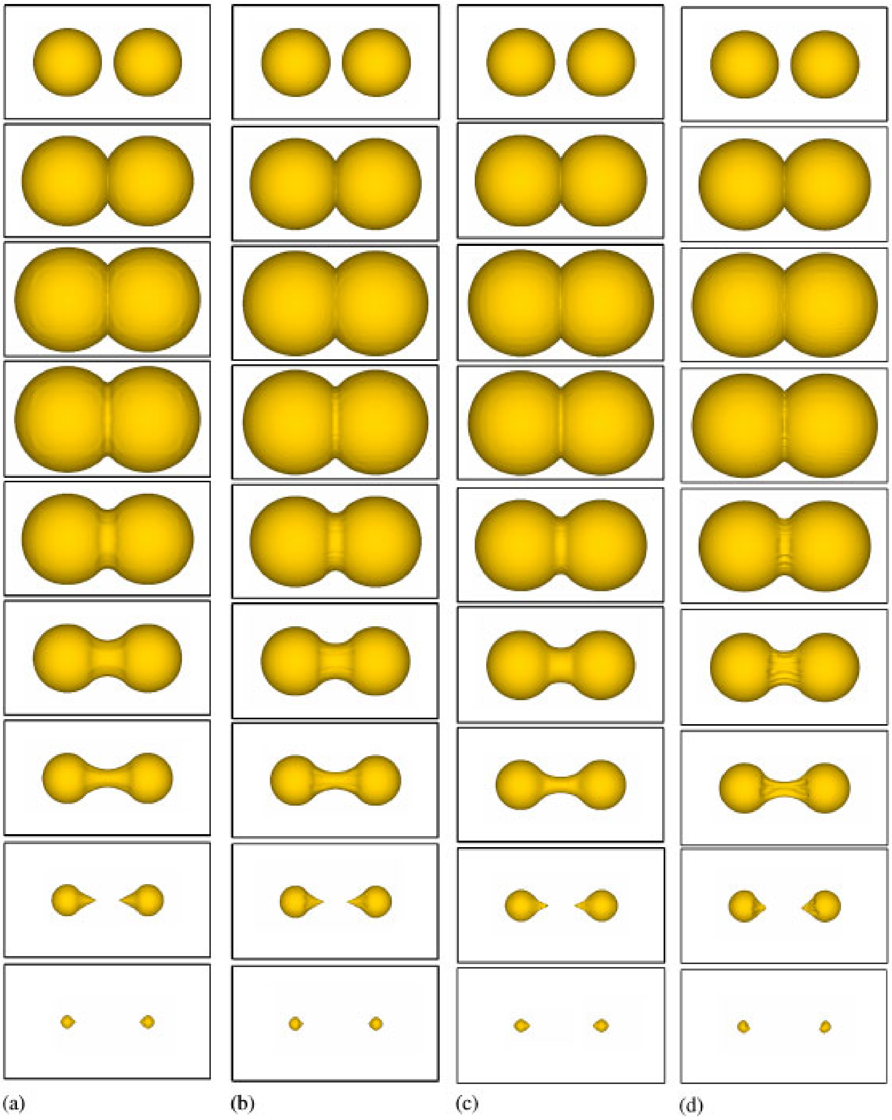

Figure 22. Coalescing and segregating spheres simulated using the MSCF1 and MSCF2 schemes on the 128^3 uniform and non-uniform grids. From top to bottom: $t=0$, $t=0.5$, $t=0.8$, $t=1.2$, $t=1.5$, $t=2.0$, $t=2.4$, $t=2.8$, $t=3.2$: (a) MSCF1, uniform grid; (b) MSCF1, non-uniform grid; (c) MSCF2, uniform grid; and (d) MSCF2, non-uniform grid.

non-uniform grids, whereas the previous schemes have difficulty even on the uniform grids. On the highly stretched non-uniform grids, the MSCF schemes are, however, also limited as they tend to be unstable. This illustrates the inherent difficulty of the sub-cell-fix approach in general.

ACKNOWLEDGEMENTS

This work was sponsored by the Swedish Research Council VR, SSF, and STEM through CeCOST. M. B. Sun was sponsored by China Natural Science Foundation (grant no. 50428605) and CSC (China Scholarship Council).

REFERENCES

1. Osher S, Fedkiw R. *Level Set Methods and Dynamic Implicit Surfaces*. Springer: New York, 2003.
2. Markstein GH. *Nonsteady Flame Propagation*. Pergamon Press: Oxford, 1964.
3. Peters N. A spectral closure for premixed turbulent combustion in the flamelet regime. *Journal of Fluid Mechanics* 1999; **242**:611–629.
4. Nilsson P, Bai XS. Modeling turbulent premixed combustion using a level-set flamelet approach. *Experimental Thermal and Fluid Science* 2000; **21**:87–98.
5. Wang P, Bai XS. Large Eddy simulation of premixed turbulent flames using flamelet approach. *Proceedings of the Combustion Institute* 2005; **30**:583–591.
6. Sussman M, Smereka P, Osher S. A level set approach for computing solutions to incompressible two-phase flow. *Journal of Computational Physics* 1994; **114**:146–159.
7. Sussman M, Fatemi E. An efficient, interface-preserving level set redistancing algorithm and its application to interfacial incompressible fluid flow. *SIAM Journal on Scientific Computing* 1999; **20**:1165–1191.
8. Sussman M, Fatemi E, Smereka P, Osher S. An improved level set method for incompressible two-phase flows. *Computers and Fluids* 1998; **27**:663–680.
9. Losasso F, Fedkiw R, Osher S. Spatially adaptive techniques for level set methods and incompressible flow. *Computers and Fluids* 2006; **35**:995–1010.
10. Sethian JA, Smereka P. Level set methods for fluid interfaces. *Annual Review of Fluid Mechanics* 2003; **35**:341–372.
11. Karni S. Hybrid multifluid algorithms. *SIAM Journal on Scientific Computing* 1996; **17**:1019–1039.
12. Fedkiw RP, Aslam T, Merriman B. A non-oscillatory Eulerian approach to interfaces in multimaterial flows (the ghost fluid method). *Journal of Computational Physics* 1999; **152**:457–492.
13. Wang ZL, Zhou ZW. An improved level-set re-initialization solver. *Applied Mathematics and Mechanics* 2004; **25**:991–997.
14. Ni M-J, Komori S, Morley NB. Direct simulation of falling droplet in a closed channel. *International Journal of Heat and Mass Transfer* 2006; **49**:366–376.
15. Enright D, Fedkiw R, Ferziger J, Mitchell I. A hybrid particle level set method for improved interface capturing. *Journal of Computational Physics* 2002; **183**:83–116.
16. Russo G, Smereka P. A remark on computing distance functions. *Journal of Computational Physics* 2000; **163**:51–67.
17. Min C, Gibou FDR. A second order accurate level set method on non-graded adaptive cartesian grids. *Journal of Computational Physics* 2007; **225**:300–321.
18. Nilsson P, Bai XS. PDF of distance function for level-set flamelet library modelling. *International Journal for Numerical Methods in Fluids* 2003; **41**:653–673.
19. Hartmann D, Meinke M, Schröder W. Differential equation based constrained reinitialization for level set methods. *Journal of Computational Physics* 2008; **227**:6821–6845.
20. Hartmann D, Meinke M, Schroder W. Erratum to ‘Differential equation based constrained reinitialization for level set methods’ [J. Comput. Phys. 227 (2008) 6821–6845]. *Journal of Computational Physics* 2008; **227**:9696.
21. Peng D, Merriman B, Osher S, Zhao H, Kang M. A PDE-based fast local level set method. *Journal of Computational Physics* 1999; **155**:410–438.
22. Shu C-W, Osher S. Efficient implementation of essentially non-oscillatory shock-capturing schemes. *Journal of Computational Physics* 1988; **77**:439–471.
23. Shu CW. High order ENO and WENO schemes for computational fluid dynamics. In *High-order Methods for Computational Physics*, Barth TJ, Deconinck H (eds). Springer: Berlin, 1999; 439–582.
24. Dupont TF, Liu Y. Back and forth error compensation and correction methods for removing errors induced by uneven gradients of the level set function. *Journal of Computational Physics* 2003; **190**:311–324.
25. Zalesak S. Fully multidimensional flux-corrected transport algorithms for fluids. *Journal of Computational Physics* 1979; **31**:335–362.

DOI: 10.1002/fld